Role of Computed Tomography Voxel Size in Detection and Discrimination of Calcium and Iron Deposits in Atherosclerotic Human Coronary Artery Specimens

Alexander C. Langheinrich, MD,† Marian Kampschulte, MD,*† Christine Crößmann, MD,*† Regina Moritz, MD,‡ Wigbert S. Rau, MD,*† Rainer M. Bohle, MD,‡ and Erik L. Ritman, MD, PhD§*

Objective: This study evaluated the influence of voxel size on its ability to discriminate calcium from iron deposits in ex vivo coronary arteries.

Methods: Postmortem human coronary arteries underwent multislice computed tomographic scan at $(600\text{-}\mu m)^3$ voxel size to provide an index of computed tomography (CT) image noise and synchrotron-based micro-CT at $(4\text{-}\mu m)^3$ voxel size to provide data for generating a range of voxel sizes 4 to $(600\text{-}\mu m)^3$ after grayscale noise was added to the projection images before reconstruction so as to mimic the effect of retaining the same radiation exposure involved in the multislice computed tomographic scan.

Results: At voxel sizes of $(20\text{-}\mu m)^3$ or smaller, iron deposits could be identified based on CT grayscale value. Voxels of $(100\text{-}\mu m)^3$ or larger cannot resolve nor distinguish iron deposits from calcifications by virtue of CT grayscale value.

Conclusions: Clinical CT scanners cannot be expected to discriminate iron deposits from calcifications by their CT value alone in the arterial wall.

Key Words: atherosclerosis, dual-source CT, human coronary arteries, imaging, micro-CT

(*J Comput Assist Tomogr* 2009;33: 517–522)

Acute myocardial infarction is often caused by the rupture of noncalcified, advanced atherosclerotic plaques.[1] As the culprit lesion seems to be largely associated with noncalcified plaques, some characteristic other than calcification, detectable by minimally invasive means, is needed to detect plaques that might lead to acute coronary occlusion. A candidate for this detection is the presence of prior hemorrhage into the plaque. Such hemorrhage would result in micro-opacities due to the iron derived from the hemoglobin in the red blood cells. Because iron is more radiopaque than the calcium deposits, this is a candidate for discrimination of iron from calcium deposits. In the past decade, several clinical imaging techniques, especially magnetic resonance imaging[2–4] and multislice computed tomography or micro–computed tomography (CT),[5–7] have been developed and used to explore how well atherosclerotic lesions can be detected and classified in vivo or experimentally. The relation of fibrocalcified lesions, as determined by CT using the Agatston score, and cardiovascular events has been demonstrated.[8–10] However, the validity of the CT grayscale values of small opacities in the arterial wall depends in part on the partial volume effect of the detector pixel size (and CT image voxel size), x-ray beam hardening because of torso diameter, and the increased quantum noise that occurs when a voxel size is decreased without suitable increase of radiation exposure. The presence of intravascular contrast agent in the lumen may further decrease the ability to detect and distinguish iron and calcium deposits.

This study includes an attempt at quantifying the impact of voxel partial volume effect on the ability to discriminate the iron from calcium deposits in the presence of intravascular contrast medium. Micro-CT studies in atherosclerotic mice[11] have shown the ability to detect and discriminate iron and calcium deposits in the wall of the aorta, both by virtue of the size of the opacities (the area of individual iron deposits within a single CT slice being $<(100\ \mu m)^2$ and calcium deposits being $>(1000\ \mu m)^2$) and the CT gray scale of those individual deposit's opacities in that iron is more attenuating than calcium. A major difference between micro-CT and clinical CT is the ability of micro-CT to generate voxels small enough to essentially eliminate the partial volume effect, which so greatly limits clinical CT. The reason that clinical CT scanners have not been constructed to generate small voxels at the high signal-to-noise ratio comparable to micro-CT is that excessive radiation exposure would be needed, an issue that is becoming of increasing concern.[12] We added noise to the micro-CT scan projection image data before CT image reconstruction so as to simulate noise in those CT image data that would occur if the total x-ray exposure was kept constant (at the current clinical CT level) independent of the CT scan voxel resolution.

MATERIALS AND METHODS

Specimens and Image Acquisition

Samples of epicardial human coronary arteries (n = 22) were obtained from the Giessen Institute of Pathology from approved autopsy cases with coronary heart disease. The study fulfilled the ethics requirements of the State Ministry of Science and Arts. During autopsy, the left and right coronary arteries were cannulated and perfused with a solution of 0.9% normal saline and heparin until the perfusate was free of blood. A lead-containing silicon polymer (Microfil MV-122; Flow Tech, Carver, Mass) was infused into the coronary arteries at a nominal pressure of 100 mm Hg. After polymerization of the polymer, arteries were cut in tissue blocks at 2.5- to 3.5-cm intervals along the entire length of the left coronary arteries and stored in 10% neutral buffered formalin.

From the *Department of Radiology, Justus Liebig University Giessen, Giessen; †Marburg GmbH, Marburg; ‡Department of Pathology, University of Homburg/Saar, Homburg, Germany; and §Department of Physiology and Biomedical Engineering, Mayo Clinic College of Medicine, Rochester, MN.

Received for publication September 5, 2008; accepted November 10, 2008.

Reprints: Erik L. Ritman, MD, PhD, Department of Physiology and Biomedical Engineering, Alfred 2-409, Mayo Clinic College of Medicine, 200 First St SW, Rochester, MN 55905 (e-mail: elran@mayo.edu).

This investigation was supported by grants (Young Investigator Program) from the Faculty of Human Medicine of the Justus Liebig University Giessen, Giessen, Germany, and by grants EB000305 and HL65342 from the National Institutes of Health, Bethesda, MD to the Mayo Clinic College of Medicine. The use of the National Synchrotron Light Source at the Brookhaven National Laboratory and the Advanced Photon Source at the Argonne National Laboratory was supported by the Office of Basic Energy Sciences, Office of Science, U.S. Department of Energy, Washington, DC, under contract nos. DE-ACO2-98CH100886 and W-31-109-Eng-38, respectively.

Synchrotron-Based Micro-CT

The micro-CT scanner with the X2B beamline at the National Synchrotron Light Source at the Brookhaven National Laboratory[13] was used to scan human coronary artery segments. The specimen was rotated at a 360-degree angle about its central axis in 0.25-degree steps resulting in 1440 projections. The axis of rotation was aligned with and close to 1 of the lateral edges of the effective 5-mm transverse dimension of the imaging array. By stitching together (at the axis of rotation in each image), the views obtained at any one angle of view between 0 and 180 degrees with the view obtained at 180 degrees plus that angle provided an effective field-of-view of up to 9.2 mm (ie, 2300 [4 μm]^2 detector pixels) in the transverse direction and 5.2 mm

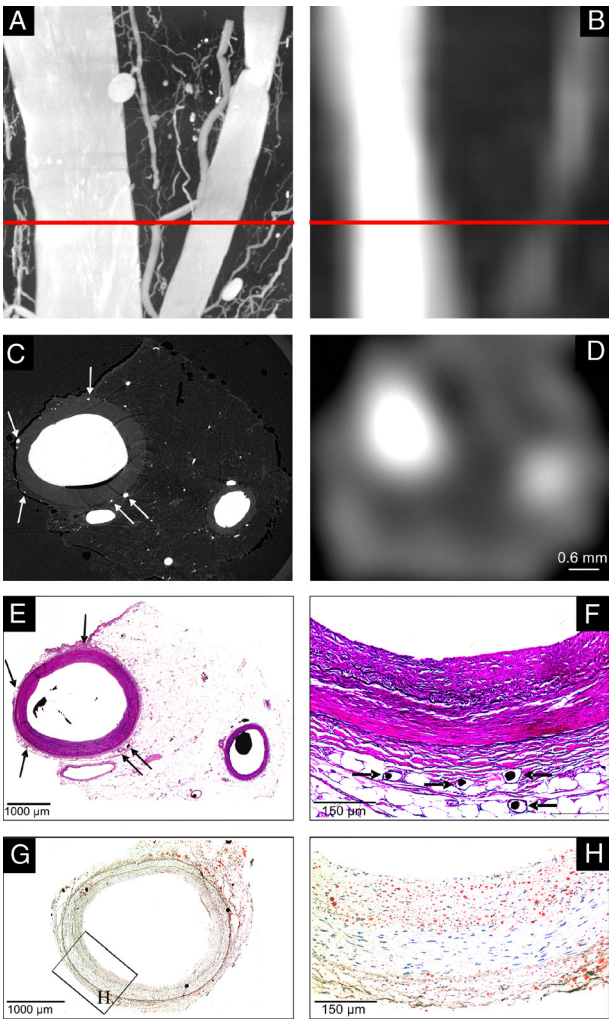

FIGURE 1. Example of a concentric, noncalcified atherosclerotic lesion visualized by synchrotron-based micro-CT imaging (A, maximum intensity projection; C, transverse single slice, 4-μm voxel size) or clinical 64-slice CT (B, maximum intensity projection; D, transverse single slice, (600-μm)^3 voxel size). The red line (A, B) indicates the location of the cross section depicted in C, D. Note that vasa vasorum are resolved in the synchrotron-based micro-CT images (C, white arrows) but not in the clinical 64-slice CT scans. The corresponding cross section of the same specimen was subsequently stained with hematoxylin and eosin with elastica counterstaining for histomicroscopical examination. Synchrotron-based micro-CT images closely matched histological microscopy (D, E). These contrast-enhanced vasa vasorum were confirmed by histologic examination (E, F, black arrows). Large lipid deposits were confirmed by histologic examination (G, magnification ×10; H, original magnification ×40; Sudan IV stain).

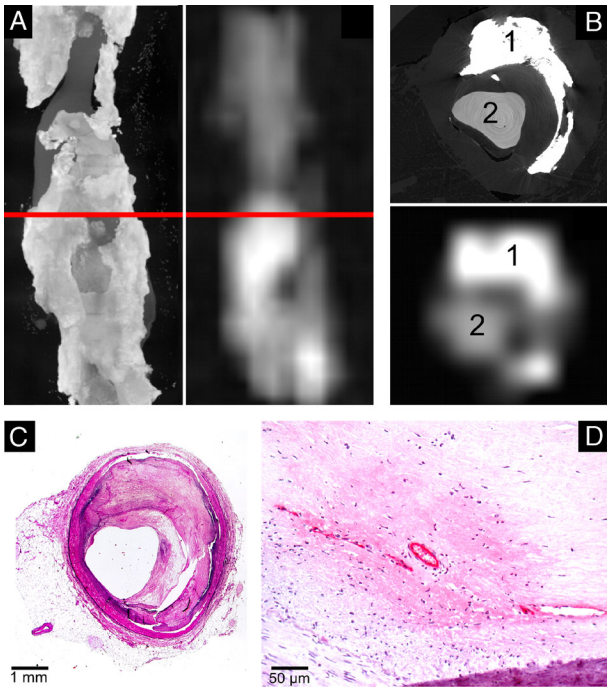

FIGURE 2. Example of a concentric, fibro-calcified atherosclerotic lesion visualized by synchrotron-based micro-CT imaging (A, maximum intensity projection; C, transverse single slice, 4-μm voxel size) or clinical 64-slice CT (B, maximum intensity projection; D, transverse single slice, 600-μm voxel size). The corresponding cross sections of the same specimen was subsequently stained with hematoxylin (F) and eosin with elastica counterstaining (E) for histological examination.

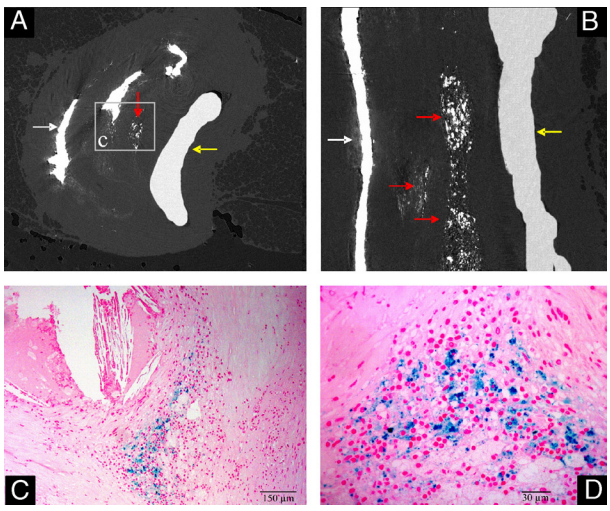

FIGURE 3. Transverse (A) and sagittal (B) synchrotron-based micro-CT images at 4-μm voxel size showed local accumulations of punctate bright spots, consistent with iron deposits resulting from individual, or small clusters of, extravascular erythrocytes. Using Perls' staining (C, original magnification ×10; D, original magnification ×40), iron deposits were confirmed.

(ie, 1300 [4 μm)^2] detector pixels) in the axial direction. Each pixel provided values with 16-bit gray scale. Samples were scanned in identical conditions with a nominal 18-keV photon energy with a 50-eV bandwidth. The (4-μm)^2 detector pixel micro-CT scan projection image data were used to also generate projection images at 12- to (600-μm)^2 pixel resolution. This involved summing the grayscale values of the appropriate number of contiguous pixels in each x-ray transmission image (ie, 3 × 3 pixels generated the (12-μm)^2 square pixel for a (12-μm)^3 voxel reconstruction and so on up to 150 × 150 pixels to make a (600-μm)^2 pixel that was then used for reconstruction of a (600-μm)^3 voxel with a 16-bit gray scale. For convenience, the cubic voxel dimensions will, from here on, be indicated by the voxel's side dimension. The gray level value of each voxel is equal to the attenuation coefficient, in 1000 per centimeter units (ie, air, 0; water, 1500). These values can be converted to Hounsfield unit (HU) by micro-CT: HU = 1000 [(micro-CT − 1500)/1500].

Noise

To mimic in keeping the total radiation exposure equal at all voxel resolutions, we added noise to the value for each pixel so that the signal value:

$$I'(n) = \sum I(j) / n^2 + 2 \times k \times RNLUT \times SQRT[\sum I(j) / n^2]$$

where I' (n) is the signal proportional to the number of photons detected by the reconfigured detector pixel consisting of n^2 4-μm pixels, $I(j)$ is the image grayscale value of the jth 4-μm pixel used to make the reconfigured n^2 pixel, and j has all integer values 1 through n^2. RNLUT is a random number look-up table ranging in value between −1 and +1. As SQRT[$\sum I(j) / n^2$] is 1 SD of the quantum noise to be expected at signal $\sum I(j)$ of the summed 4-μm pixel values, we use ±2SD to cover 95% of all possible noise values. Parameter k is a scaling factor such that the noise measured in the dual-source CT scanner's 600-μm voxel image is comparable to that in the 600-μm voxel CT image data computed from the 4-μm micro-CT image data (ie, k = Noise in 64-slice image / (2 × RNLUT × SQRT[$\sum I(j) / 150^2$]). By adding this noise, the comparison of different voxel sizes now includes the increased noise with decreased voxel size that results from keeping the total x-ray exposure constant regardless of voxel size.

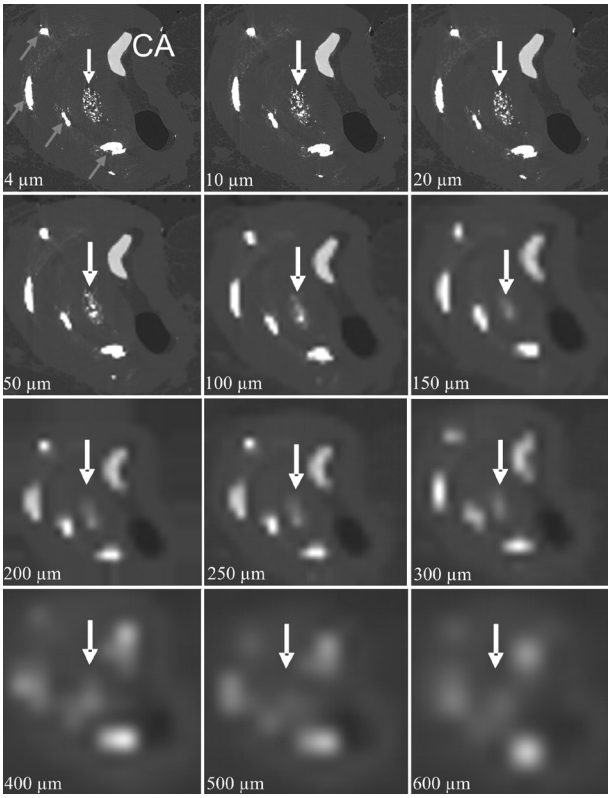

FIGURE 4. Transverse, single slice synchrotron-based micro-CT images at resolutions from 4- to 600-μm voxel size demonstrating an advanced atherosclerotic lesion. Calcifications (gray arrows) are spatially separated from iron deposits (white arrow) and contrast-enhanced lumen (CA). At 100-μm voxel size, the punctate bright spots are blurred owing to partial volume effect so that the gray scale is sufficiently reduced to the extent that they cannot be differentiated from calcifications.

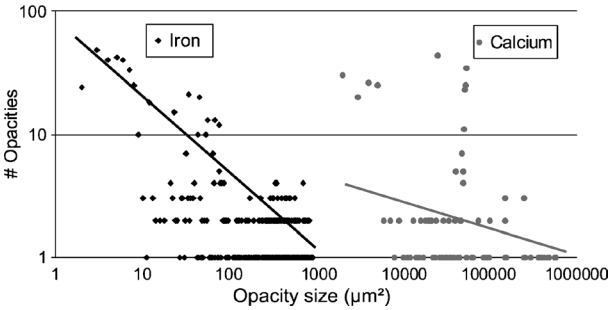

FIGURE 5. Frequency histogram of different-sized opacities within the synchrotron micro-CT images of the human coronary arteries demonstrates differences in spot size distribution ($P < 0.001$) between iron and calcium deposits in advanced atherosclerotic lesions. The linear log/log relationship of the iron deposits is consistent with a random spatial distribution of small opacities, whereas the lack of that relationship for the calcifications suggests nonrandom spatial distribution of the deposits.

64-Slice CT Scan Protocol

All arteries were also scanned with a 64-slice CT scanner equipped with a z-axis flying focus technology (Definition; Siemens, Erlangen, Germany) at 120 kilovolt (peak) (kV[p]) and at 250 milliampere second with an aluminum filter.[14] The voxel size used was 0.6 mm^3.

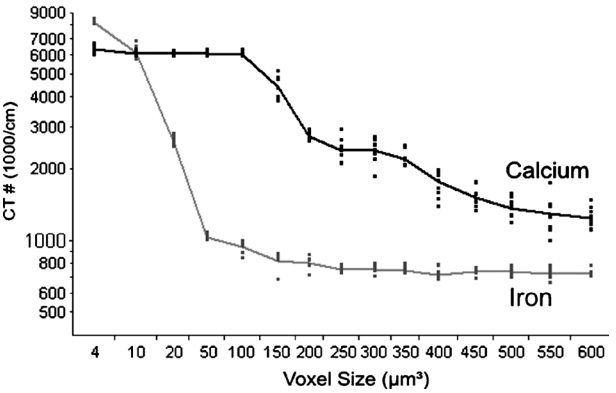

FIGURE 6. This is a log/log plot of the CT value of iron and calcium obtained at different scanner resolutions (4- to 600-μm voxel size). Note the decreasing CT number of the punctate iron deposits crossing the calcium CT value at 12-μm voxel resolution due to blurring partial volume effects.

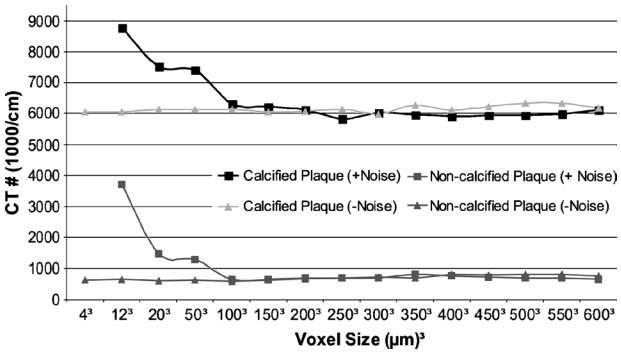

FIGURE 7. The sum of all the CT grayscale values (above the tissue background grayscale value) in a plaque region, instead of the average CT grayscale value of a plaque region, remains essentially constant regardless of voxel size except for the smallest voxels where noise spikes now can produce very high grayscale values.

Grayscale Measurements

Grayscale values of voxels within the region of interest within slices at 600-μm intervals along the artery sample (ie, approximately 80 per coronary artery sample) in the micro-CT and 64-slice CT images were established using the ANALYZE image analysis software program (Analyze 6.0; Mayo Clinic College of Medicine, Rochester, MN).

Histology

After completion of the CT scans, the specimens were embedded and sectioned for histopathological analysis of the atherosclerotic lesions. Serial sections at 3-mm intervals were stained with hematoxylin and elastica (each n = 9 per artery). Contiguous sections were prepared to identify iron (Perls' stain). Cross sections were digitized and analyzed by 2 experienced pathologists in consensus (R.M.B. and R.M.). Histological plaque characterization was blinded to the results of the micro-CT image analysis.

Statistical Analysis

All data are presented as mean (SD) for all arteries. Statistical analysis was performed using JMP 5.1 (SAS Institute, Cary, NC). One-way analysis of variance, followed by a Tukey-Kramer post hoc test with correction for multiple comparisons, was used to identify the statistical differences among the measurements.

Individual comparison was performed by an unpaired Student *t* test. $P < 0.05$ was considered significant in all analyses.

RESULTS

As illustrated in Figures 1 and 2, synchrotron-based micro-CT images closely match histological microscopy and that at 4-μm voxel size, plaque details are clearly visualized but not at the 600-μm voxel size. The 600-μm voxel micro-CT images closely mimic the limitations of clinical CT scanners for plaque visualization and classification.

Iron and Calcium Deposits

As illustrated in Figure 3, synchrotron-based micro-CT images at 4-μm voxel size showed local accumulations of punctate bright spots, consistent with iron deposits resulting from individual extravascular erythrocytes. The presence of iron in hemorrhaged lesions (American Health Association classification type VIb) was confirmed by histological examination using Perls' staining. Those bright spots are spatially separated from calcifications as demonstrated in Figures 3 and 4.

Figure 5 shows that the iron and calcium opacities visualized within the synchrotron micro-CT images of advanced

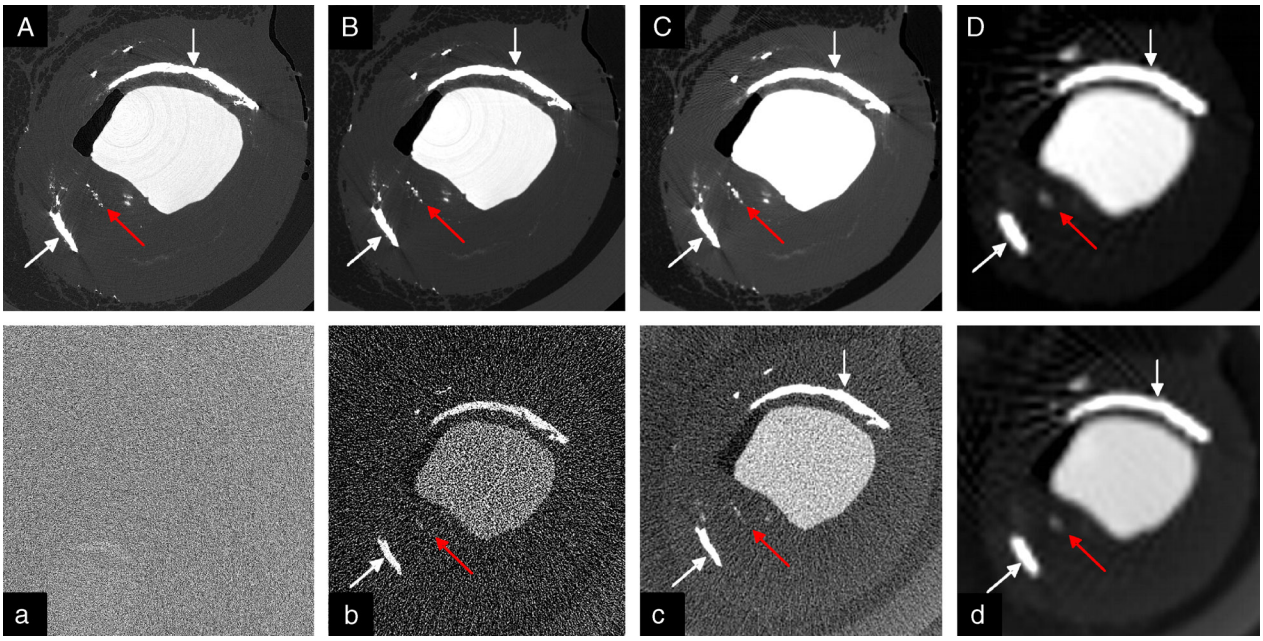

FIGURE 8. Transverse, single slice synchrotron micro-CT at 4- (A, a), 12- (B, b), 20- (C, c), and 100- (D, d) μm voxel size without (A, B, C, D) and with noise added (a, b, c, d). Calcifications (white arrows) and iron deposits (gray arrow) are discriminated from the contrast-enhanced lumen. This noise renders the small voxel images at 4-μm voxel size useless as vessel wall cannot even be distinguished. At 100-μm voxel size (D, d), the image quality is comparable.

atherosclerotic lesions in human coronary arteries are very different in size distributions ($P < 0.001$).

Iron deposits can be visualized and classified using the grayscale values using synchrotron-based micro-CT up to 12-μm voxel size. In images with voxels greater than 20 μm, the punctate bright spots are sufficiently blurred by the partial volume effect that they cannot be differentiated from calcifications by virtue of their grayscale value as shown in Figure 6.

Noise

When simulating the noise resulting from maintaining the total x-ray exposure at the clinical level, regardless of voxel size, neither the iron nor the calcifications are visible at 4-μm voxel resolution (Figs. 7 and 8).

DISCUSSION

The present study demonstrates that high-resolution micro-CT imaging allows detection and discrimination of atherosclerotic plaque components such as iron and calcium by virtue of the different sizes of the individual iron and calcium deposits and by their individual CT grayscale values. At present, detailed plaque characteristics, especially markers of plaque vulnerability such as neovascularization and hemorrhage,[15] are not reliably identifiable with voxel resolutions achievable with current clinical CT scanners. The 3D images generated from the micro-CT image data, without noise added, show essentially only the effect of partial volume because of large voxels. If the signal-to-noise ratio is maintained independent of voxel size (ie, if the radiation exposure increases inversely with the volume of the voxel)[16,17] the impact of this noise on the ability to detect and quantitate opacities in the arterial wall is significant, relative to the partial volume effect as shown in Figure 8. Thus, where the partial volume effect is due to the dilution of the signal, the noise obscures the signal. Rose[18] showed that a given change in image brightness (the signal), from one pixel to another, can be unequivocally detected if that change is at least 5 times larger than the noise in the signal. Thus, it is to be expected that if x-ray exposure is kept at current whole-body CT levels, the CT images cannot provide the voxel resolution needed to discriminate iron deposits from calcium deposits on the basis of opacity size, nor of their different inherent radiopacity. Up to now, data of different lesion types obtained from clinical CT scanners were limited to the classification of either lipid-rich, fibrous (intermediate), or calcified, indicating the difficulties in exact classification of different advanced lesion types. Because advanced noncalcified atherosclerotic lesions become vascularized by newly formed vasa vasorum, intraplaque hemorrhage may be more likely and may therefore be a marker of plaque vulnerability.[19]

Limitations

This study addresses only the role of voxel size in CT-based detection and discrimination of calcium from iron deposits in atheromatous plaques. Issues such as x-ray beam hardening due to surrounding thoracic tissues, motion of the heart, and the angle of the blood vessel lumen to the scan plane (ie, more partial volume effects of lumen contrast agent and arterial wall) are not addressed. The micro-CT image scans were performed at 18 keV to provide the approximately 10% transmission needed for optimal CT imaging. Thus, the attenuation mechanism is predominantly photoelectric, whereas the clinical CT scan at 120 kVp is predominantly Compton scatter–based. Moreover, the 120-kV spectrum ranges from 40 to approximately 120 keV, which results in considerable beam hardening, which also impacts on the CT image grayscale values. However, the partial volume effect is also mediated by the location of the voxel relative to anatomical borders of the arterial wall with the arterial lumen (especially if there is contrast medium in the blood) and with surrounding tissues (especially adipose tissue).

Clinical Implications

We conclude that if clinical CT is to be used to detect and discriminate calcium from iron deposits in atherosclerotic plaques then voxels no larger than 100 μm (ie, 0.001 mm^3) will be needed. If iron deposits can be identified and quantitated, it may be possible to identify intraplaque hemorrhage. Consequently, the combined imaging of plaque perfusion (as an index of vasa vasorum density) and plaque iron deposits may form a basis for CT imaging–based identification of vulnerable plaques. However, as even monochromatic x-ray alone would not be able to distinguish between iron and calcium by virtue of their different x-ray attenuation coefficients at voxel sizes larger than 100 μm, dual-energy CT scanning should be explored as a means of distinguishing iron and calcium deposits.

ACKNOWLEDGMENTS

We would like to thank David F. Hansen, Diane R. Eaker, Andrew J. Vercnocke, and Steven M. Jorgensen of the Mayo Clinic College of Medicine and Gunhild Martels of Justus Liebig University Giessen for their technical assistance.

REFERENCES

1. Burke AP, Virmani R. Pathophysiology of acute myocardial infarction. *Med Clin North Am*. 2007;91:553–572.
2. Canet-Soulas E, Letourneur D. Biomarkers of atherosclerosis and the potential of MRI for the diagnosis of vulnerable plaque. *MAGMA*. 2007;20:129–142.
3. Kramer CM, Anderson JC. MRI of atherosclerosis: diagnosis and monitoring therapy. *Expert Rev Cardiovasc Ther*. 2007;5:69–80.
4. Lipinski MJ, Amirbekian V, Frias JC, et al. MRI to detect atherosclerosis with gadolinium-containing immunomicelles targeting the macrophage scavenger receptor. *Magn Reson Med*. 2006;56:601–610.
5. Becker CR. Assessment of coronary arteries with CT. *Radiol Clin North Am*. 2002;40:773–777.
6. Johnson TR, Nikolaou TR, Busch S, et al. Diagnostic accuracy of dual-source computed tomography in the diagnosis of coronary artery disease. *Invest Radiol*. 2007;42:684–691.
7. Langheinrich A, Bohle RM, Greschus S, et al. Atherosclerotic lesions at micro CT: feasibility for analysis of coronary artery wall in autopsy specimens. *Radiology*. 2004;231:675–681.
8. Arad Y, Goodman KJ, Roth M, et al. Coronary calcification, coronary disease risk factors, C-reactive protein, and atherosclerotic cardiovascular disease events: the St. Francis Heart Study. *J Am Coll Cardiol*. 2005;46:158–165.
9. Hoffmann U, Kwait DC, Handwerker J, et al. Vascular calcification in ex vivo carotid specimens: precision and accuracy of measurements with multi-detector row CT. *Radiology*. 2003;229:375–381.
10. Hong C, Becker CR, Schoepf UJ, et al. Coronary artery calcium: absolute quantification in nonenhanced and contrast-enhanced multi-detector row CT studies. *Radiology*. 2002;223:474–480.
11. Langheinrich AC, Michniewicz A, Sedding DG, et al. Quantitative x-ray imaging of intraplaque hemorrhage in aortas of apoE(−/−)/LDL(−/−) double knockout mice. *Invest Radiol*. 2007;42:263–273.
12. Brenner DJ, Hall EJ. Computed tomography—an increasing source of radiation exposure. *N Engl J Med*. 2007;357:2277–2284.

13. Ritman EL, Jorgensen SM, Lund PE, et al. Synchrotron-based micro-CT of in situ biological basic functional units and their integration. *Proc SPIE, Dev X-Ray Tomogr*. 1997;3149:13–24.
14. Flohr TG, Stierstorfer K, Ulzheimer S, et al. Image reconstruction and image quality evaluation for a 64-slice CT scanner with *z*-flying focal spot. *Med Phys*. 2005;32:2536–2547.
15. Virmani R, Kolodgie FD, Burke AP, et al. Atherosclerotic plaque progression and vulnerability to rupture: angiogenesis as a source of intraplaque hemorrhage. *Arterioscler Thromb Vasc Biol*. 2005;25: 2054–2061.
16. Chesler DA, Riederer SJ, Pelc NJ. Noise due to photon counting statistics in computed x-ray tomography. *J Comput Assist Tomog*. 1977;1:64–74.
17. Grodzins L. Electron, proton and photon induced x-ray microprobes: analytic sensitivity versus spatial resolution. *Neurotoxicology.* 1983;4:23–33.
18. Rose A. Sensitivity performance of the human eye on an absolute scale. *J Opt Soc Am*. 1948;31:196–199.
19. Heistad DD. Unstable coronary-artery plaques. *N Engl J Med*. 2003; 349:2285–2287.